Eur. Phys. J. B **3**, 455–461 (1998)

THE EUROPEAN PHYSICAL JOURNAL B

Optical response of thin plasma-polymer films with non-spherical silver nanoparticles

A. Heilmann[1,2,a], M. Quinten[1,2], and J. Werner[1]

[1] TU Chemnitz, Institut für Physik, 09107 Chemnitz, Germany
[2] RWTH Aachen, I. Physikalisches Institut, 52056 Aachen, Germany

Received: 23 July 1997 / Revised: 27 October 1997 / Accepted: 3 December 1997

Abstract. The size and shape of silver nanoparticles which are embedded in a plasma-polymer matrix were obtained by transmission electron microscopy and analyzed with optical image processing. We used a sample in which silver particles were present before and after reshaping caused by thermal annealing in adjacent regions. As most of the particles appeared as elongated rotational ellipsoids, the major and minor half axis were determined for each particle. We adopted the model of Gans in the Rayleigh approximation to calculate for each investigated particle the extinction spectra from 4000 cm^{-1} to 35 000 cm^{-1} using the data from the image processing. The various spectra for 368 silver particles were added to get total extinction spectra for the sample as deposited and after reshaping, respectively. We found good agreement with the experimental spectra. The blue shift of the plasma-resonance absorption, which occurs due to the reshaping of the silver particles during thermal annealing, was also confirmed by using only changes in the particle sizes and shapes.

PACS. 78.66.Vs Microparticles – 61.46.+w Clusters, nanoparticles, and nanocrystalline materials – 81.05.Zx New materials: theory, design, and fabrication

1 Introduction

It is well-known that the electrical and optical properties of nanostructural granular materials are determined by their microstructure. For insulators with embedded metal particles, the optical properties are mainly determined by the size and shape of the embedded particles. For description of the optical properties with consideration of the microstucture, it is necessary to find an appropriate theoretical model and to select samples which allow microstructural investigations and optical measurements as well. For the latter, plasma-polymer thin films with embedded metal nano-particles are well-suited. Besides, in addition to the application range of plasma-polymer films [1], plasma-polymer films with embedded metal particles open new fields of applications *e.g.* for optoelectronic materials, as resist materials for electron-beam lithography, or as intermediate layers for adhesion improvement [2–4].

In such nanocomposite materials, the size and shape of the embedded metal particles can be determined very effectively with transmission electron microscopy (TEM). Moreover, the size and shape of the nanoparticles can be artificially modified by thermally induced processes like reshaping, coalescence, as well as Ostwald ripening [5,6] without destroying the polymer matrix. These processes can be caused by laser irradiation [7–9] or by electron-beam irradiation [10,11], the latter having the advantage that the microstructural changes can be limited to very small substrate areas.

The optical properties of metal nanoparticles are determined by a collective oscillation of the free electrons in the particles which is mostly described by the term plasma-resonance absorption and can be observed by conventional spectroscopy. The plasma-resonance absorption depends on the particle material and on the particle size and shape. Furthermore, it is influenced by the dielectric constant of the host medium [12]. Different models can be used to describe these dependences. The first attempt is to use effective medium theories (for a review see [12]) in which the dielectric constant of the inhomogeneous film is approximated by a mixing of the dielectric constants of the particles and of the matrix material. The modelling of plasma-polymer films with embedded silver particles with effective medium theories already gives reasonable results [5], even though in all these effective medium theories the size and shape of the particles enter the calculation only as mean values.

Another theoretical route is the calculation of the optical properties of single metal particles with the Mie theory [13]. However, the Mie theory is only valid for spherical

[a] *Present address:* Fraunhofer Institute of Mechanics of Materials, Branch Laboratory for Microstructure of Materials and Systems, 06120 Halle, Heideallee 19, Germany.
e-mail: `hei@iwmh.fhg.de`

particles, it cannot be used for nonspherical particles. For nonspherical particles various attemps were made [14], the most prominent, perhaps, being the model of Gans [15] for ellipsoidal particles. This model is only valid for particles in the Rayleigh approximation, *i.e.*, for particles small compared to the wavelength of the incident light. In this paper, we use the Rayleigh-Gans model for successful interpretation of optical extinction spectra measured on plasma-polymer films with embedded silver nanoparticles. According to the assumption of elongated spheroidal particles, extensive image analysis of transmission electron micrographs was made to determine the length of the major and minor axis of the as-deposited and annealed particles.

The paper is organized as follows. Section 2 describes the preparation of plasma-polymer films with embedded silver nanoparticles and the determination of the microstructure which was locally changed by electron-beam irradiation and *in situ* thermal annealing. In Section 3, the results of TEM-analysis and optical image processing of TEM-micrographs are presented. Then, measured optical extinction spectra are shown, followed by a brief introduction into the Rayleigh-Gans model. Finally, results from this theory are compared to the measured spectra and discussed. Section 4 gives some summarizing conclusions.

2 Experimental

Plasma-polymer thin films with embedded silver particles were deposited by simultaneous plasma-polymerization and metal evaporation in a deposition reactor described in [16]. The film used for this investigation was deposited from the monomer benzene (C_6H_6) at room temperature. The plasma-polymerization power density was 0.15 W cm^{-2} at a monomer flow rate without inert gas of 0.1 Pa l s^{-1}.

The metal-containing plasma-polymer films were deposited as multilayer systems with metal particles only in one plane between two plasma-polymer layers. Electron micrographs of these multilayer systems showed well-separated single particles, which is advantageous for determination of particle sizes and shapes. The vertical structure of the multilayers was examinated by cross-sectional transmission electron microscopy (XTEM) [17] and XPS depth profiling [18], confirming that the metal particles are actually situated in one plane. Together with TEM-micrographs in lateral direction, the size and shape of the particles in all three dimensions can be determined [17].

For the experiments presented in this paper, graphite coated copper grids for TEM investigation and quartz slides for optical measurements were used as substrates. The thickness $d = 100$ nm of the prepared film was determined by interferometry after deposition on the quartz substrates.

Electron microscopy was carried out using a Philips electron microscope CM 20 FEG at 200 kV acceleration voltage. For *in situ* annealing a sample heating unit was used.

The sizes and shapes of the embedded particles can be varied during film deposition. They mainly depend on the amount of evaporated metals, the pressure during deposition, and the distance of the sample from the metal evaporation source. As shown formerly [5], the particles have a broad size distribution which can be described in principle with a logarithmic-normal distribution. Furthermore, for samples with mean particle sizes larger than ≈ 5 nm deviations from the spherical shape cannot be neglected.

At moderate thermal annealing much below the melting point of the metal particles, substantial changes of the size and shape of the particles were observed [5,20, 21]. Diffusion processes occur along the grain boundaries and the particle surface (reshaping). If two neighbouring particles are closely connected, the particles coalesce and the number of the embedded particles decreases. Moreover, also hints of diffusion of metal atoms through the polymer matrix (Ostwald ripening) were found [6].

If the sample is annealed inside the electron microscope, changes in the particle size and shape can be observed *in situ* [22]. However, during thermal annealing inside the electron microscope, contamination of the sample especially at the irradiated part was found [19], causing hardening of the polymer matrix. Then, the thermally induced reshaping of the metal particles takes place at higher temperatures compared to the unirradiated parts of the samples. So, the present state of the deposited microstructure is *frozen* at the irradiated part of the sample, while it changes in the other parts during annealing.

Extinction spectra were measured with a commonly used spectrophotometer in the spectral region between 4000 cm^{-1} and 50 000 cm^{-1} before and after thermal annealing. Annealing of the optical samples was done under high vacuum conditions (10^{-4} Pa) with a heating rate of about 3 K min^{-1} up to 480 K.

3 Results

3.1 Particle size and shape

Figure 1 depicts a TEM-micrograph of a sample prepared as described above and treated with electron-beam irradiation and *in situ* annealing in the electron microscope. The electron-beam was placed on the left part of the sample (left part of Fig. 1a) during annealing. The maximum temperature on the sample holder was 770 K, but due to the low thermal conductivity of the sample, we suppose that the real temperature at the investigated sample region was lower. Because of contamination and hardening of the polymer matrix by electron-beam irradiation during the thermal annealing, the microstructure of the irradiated sample part has remained as deposited, also after thermal annealing. The right part of Figure 1a shows the microstructure of the sample part without electron-beam irradiation during thermal annealing. At this sample part, thermally induced reshaping of the silver particles took place. So, Figure 1a gives the silver particle sizes

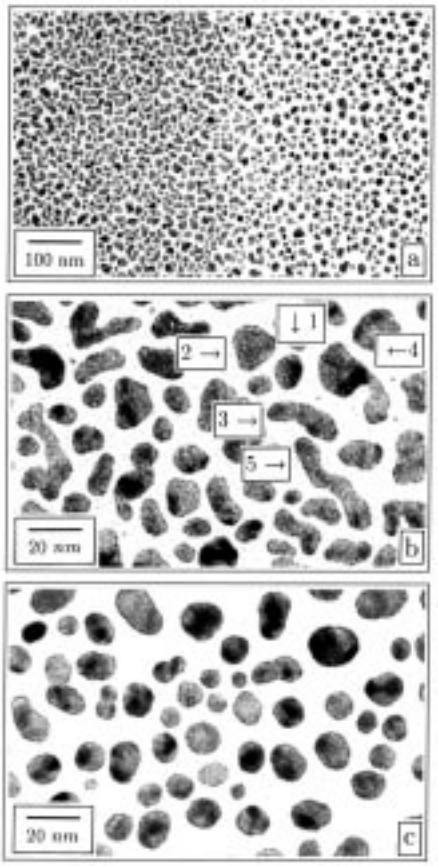

Fig. 1. TEM micrographs of embedded particles. Figure 1a shows a sample part before (left) and after (right) reshaping and coalescence. Details are given in the text. The other TEM micrographs are section enlargments from the left part (Fig. 1b) and the right part (Fig. 1c) of Figure 1a.

and shapes before (left) and after (right) reshaping. Figures 1b and 1c are section enlargements from the left and right part of Figure 1a, respectively.

The substantial changes in the particle sizes and shapes are due to thermal induced grain boundary diffusion as well as surface diffusion of silver atoms which results in a recrystallization and reshaping of the silver particles, discussed in more details in reference [6].

To get quantitative results on the size and shape distribution of the embedded particles, TEM-micrographs were analysed with an optical image processing system (Kontron KS 400). The TEM-micrograph from Figure 1 was scanned with a CCD camera and transfered into a digital image with a size of 784×600 pixels, using several image improvement routines. Based on the pixel coordinates of the digital image, area (Ar) and perimeter (U) as well as the center of gravity of each particle were calculated.

For approximately spherical particles, the particle size D is given as the mean value of 36 lines of intersections (ferets) F_n as particle projections at different angles $D = \frac{1}{36}\sum_{n=1}^{36} F_n$. For particles with large deviations from the spherical shape, additionally the shape factor $S = \frac{4\Pi Ar}{U^2}$ or the aspect ratio $R = \frac{F_{min}}{F_{max}}$, where F_{min} and F_{max} represent the minimal and maximal feret, can be used for particle form characterization [23].

Table 1. Values for the major axis A and the minor axis B of five selected particles.

Particle	major axis A	minor axis B
1	9.7 nm	7.3 nm
2	12.1 nm	11.0 nm
3	21.0 nm	7.0 nm
4	23.6 nm	13.1 nm
5	33.9 nm	6.8 nm

In this paper, also with respect to the results of the XTEM examination [17], we assume the particles to be elongated spheroids (rotationally symmetric ellipsoids), which are described by the mean half axis A (major axis) and the lower half axis B (minor axis). The values for A and B were determined from image processing. As an example, the major axis A and the minor axis B for five representative particles selected from Figure 1b are summarized in Table 1.

In total, 368 particles were analyzed, both, before and after annealing, and the results are given in three-dimensional histograms (Fig. 2). The x-direction gives the minor axis B, the y-direction the major axis A and the z-direction the number of particles found in the A-B-interval (count). Figure 2a shows the histogram for the sample as deposited and Figure 2b for the annealed sample. Especially at Figure 2a there is an important number of large particles, with an eccentricity $e = B/A \ll 1$. The particle size and shape distribution from Figure 2a was determined by the film deposition and it is typical for silver particles embedded in a plasma-polymer thin film matrix [23]. Obviously, as a result of thermal induced reshaping and recrystallization the eccentricities of the particles have increased and the particle shapes gets closer to the spherical shape ($A = B$) when the sample was annealed.

3.2 Optical properties

Small noble-metal nanoparticles which are embedded in a surrounding non-absorbing matrix exhibit optical plasma-resonance absorption [12]. Spectral position, halfwidth, and intensity of the optical absorption strongly depend on the particle size and shape, and on the dielectric properties of the particle material and the surrounding medium. Therefore, if the particle size and shape change due to thermal annealing, changes of the plasma-resonance absorption can be expected. For silver particles embedded in a plasma-polymer matrix, a shift of the resonance position to higher wavenumbers (blue shift) and a decrease of the halfwidth of the plasma-resonance absorption were found [5,18,24], which were correlated not only with changes of the particle sizes but also with changes of the particle shapes.

For the sample under consideration, in Figure 3 the optical extinction spectra before and after thermal annealing

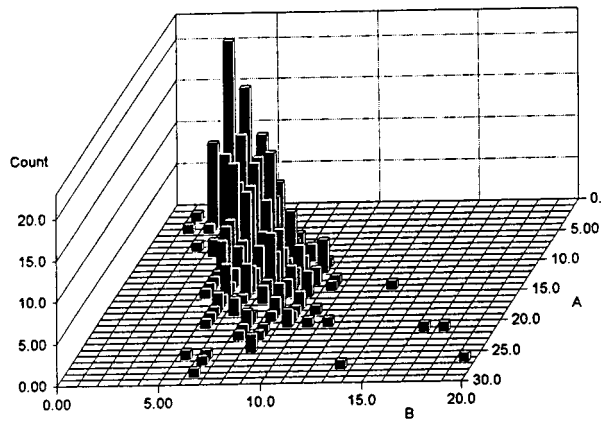

(a)

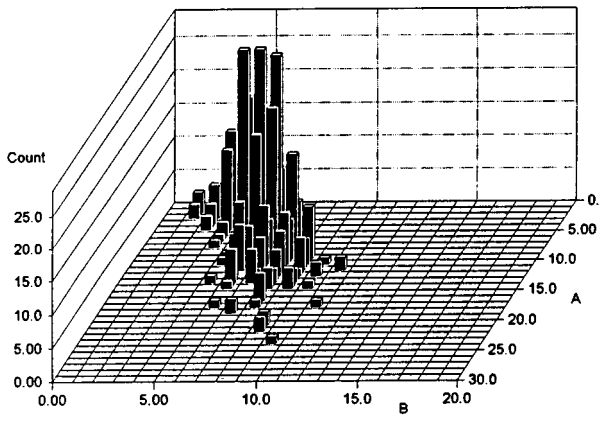

(b)

Fig. 2. Three-dimensional particle histograms of the minor axis (B), the major axis (A), and the number of particles found in the A-B-interval. Figure 2a belongs to the left part and Figure 2b to the right part of Figure 1a.

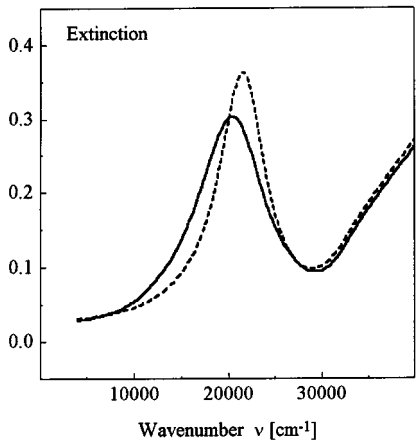

Fig. 3. Measured extinction spectra of embedded silver particles before (solid line) and after (dashed line) thermal annealing (480 K).

are plotted. The microstructure corresponds to that on the micrograph of Figure 1. The plasma-resonance absorption is peaked at $\tilde{\nu}_r = 20\,410$ cm^{-1} before annealing and at $\tilde{\nu}_r = 21\,740$ cm^{-1} after annealing. That means that the extinction peak shifts with $\Delta\tilde{\nu}_r = 1330$ cm^{-1} to higher wavenumbers. In addition, the halfwidth of the plasma-resonance absorption, which was determined by Lorentz peak fitting, decreases from $\Gamma = 5450$ cm^{-1} to $\Gamma = 4130$ cm^{-1}.

In former works, optical properties of plasma-polymer thin films with embedded silver particles were described with different effective medium theories, in particular with the Maxwell-Garnett theory [25] and its extension to ellipsoidal particles [24,26] or with the Bergman theory [23] as well. The blue shift which occurs at thermal annealing was reproduced using the extension of the Maxwell-Garnett theory for parallel oriented ellipsoidal particles, under consideration of different depolarisation factors [5]. However, as in the effective medium theory the depolarisation factor can only be used as mean value for all particles, we prefer here to compute optical spectra of typical single particles as characterized with the image processing and to sum up all contributions to a complete spectrum.

As only for a few geometrical bodies rigorous solutions for the extinction and scattering of particles are available (spheres: Mie theory [13], spheroids: [28], infinite cylinder [29,30]), the spectra of other particles must be described using approximations. In the Rayleigh approximation, Gans [15] developed a model for ellipsoidal particles and Fuchs [31] a model for cubic particles. Both are based on the calculation of a dipole polarizability of the particle. We used the model of Gans to determine the extinction of the nonspherical particles in the plasma-polymer film. In the following section, the theory will be briefly introduced and computational results are presented.

3.3 Computational results

In the Rayleigh approximation the particle is so small that an applied electric field $\mathbf{E}_0$ only induces a dipole of moment $\mathbf{p}$ in the particle. In general, $\mathbf{E}_0$ and $\mathbf{p}$ are not collinear, meaning that the polarizability $\hat{\alpha}$ of the particle is a tensor:

$$\mathbf{p} = \epsilon_0\ \epsilon_m\ \hat{\alpha}\ \mathbf{E}_0. \tag{1}$$

In this notation, the elements of the polarizability tensor are only proportional to the particle volume, similar to the atomic polarizability. ϵ_m is the dielectric constant of the surrounding medium. A dipole with linear response oscillates with the same frequency as the applied electric field and, hence, emits an electric field $\mathbf{E}_s$ asymptotically given in the far field by

$$\mathbf{E}_s = \frac{e^{ikr}}{ikr}\frac{ik^3}{4\pi\epsilon_0\epsilon_m}\mathbf{e}_r \times (\mathbf{e}_r \times \mathbf{p}). \tag{2}$$

Using Poynting's theorem, and after some mathematics, the extinction cross section C_{ext} for the dipole is finally

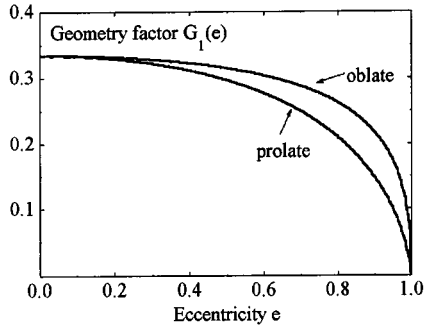

Fig. 4. Geometry factor $G_1(e)$ as function of the eccentricity e.

obtained as

$$C_{ext} = k\ \Im \sum_{i=1}^{3}\sum_{j=1}^{3} \alpha_{ij} e_i e_j, \tag{3}$$

$\Im$ means the imaginary part, and e_i and e_j are the normalized components of the incident field vector. For an ellipsoidal particle with three different elementary axes A, B and C, the polarizability tensor only has diagonal elements α_{jj}, with

$$\alpha_{jj} = 4\pi\ ABC \frac{\epsilon(\omega) - \epsilon_m(\omega)}{\epsilon_m(\omega) + G_j[\epsilon(\omega) - \epsilon_m(\omega)]}\,. \tag{4}$$

G_j are factors taking into account the geometry of the ellipsoid. They satisfy the conditions

$$\sum G_j = 1, \qquad G_j \leq 1 \qquad \forall j. \tag{5}$$

For comparison with our experiments, the special case of spheroids has been found suitable. They are characterized by coincidence of two of the three elementary axes. One distinguishes elongated or prolate spheroids with $B = C$, and flatened or oblate spheroids with $A = B$. In the following, A is always the major axis and B the minor axis of the spheroid. Accordingly, only two factors $G_1(e)$ and $G_2(e)$ are relevant, depending on the eccentricity e, defined for a spheroid as

$$e^2 = 1 - \left(\frac{B}{A}\right)^2. \tag{6}$$

G_1 differs for prolate and oblate spheroids:

$$\text{prolate:} \quad G_1(e) = -g(e)^2 \left\{1 - \frac{1}{2e} \ln\left(\frac{1+e}{1-e}\right)\right\} \tag{7}$$

$$\text{oblate:} \quad G_1(e) = \frac{g(e)}{2e^2}\left\{\frac{\pi}{2} - \tan[g(e)]^{-1}\right\} - \frac{g(e)^2}{2} \tag{8}$$

with

$$g^2(e) = \frac{1-e^2}{e^2}\,. \tag{9}$$

In Figure 4, $G_1(e)$ is plotted *versus* the eccentricity e for both prolate and oblate spheroids. It starts with $G_1(0) = 1/3$, which is the case of a spherical particle ($A = B = R$) and decreases with increasing eccentricity. *Vice versa*, following equation (5), $G_2(e)$ also starts with $G_2(0) = 1/3$, but it increases with increasing eccentricity. It follows now from equation (4) that for a spheroidal silver particle two surface plasma-resonances are induced, namely, when the optical constants of silver satisfy the conditions

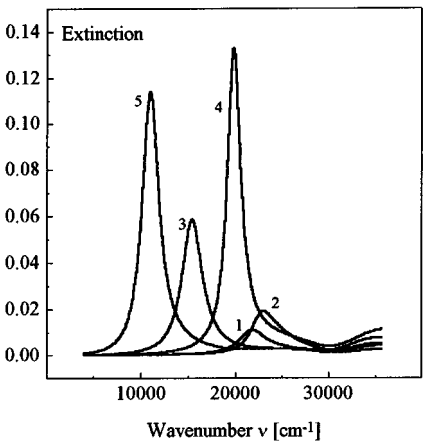

Fig. 5. Computed extinction spectra (Eq. (7)) for particles 1 through 5 from Figure 1b.

$$\epsilon(\omega) = -\epsilon_m \frac{1 - G_j}{G_j}\,. \tag{10}$$

For simplicity, consider the dielectric constant to be purely a Drude dielectric constant without damping, *i.e.*

$$\epsilon(\omega) = 1 - \frac{\omega_p^2}{\omega^2} \tag{11}$$

with ω_p being the plasma frequency of the free electrons. Then, it becomes obvious that the plasma-resonance for G_1 contributes to the spectrum at lower frequencies, the plasma-resonance for G_2 contributes at higher frequencies than the frequency at which the plasma-resonance of the equivalent volume sphere with $G_1 = G_2 = 1/3$ is peaked.

3.4 Optical calculations

Optical extinction spectra for prolate spheroids were computed using the optical constants of silver from [32], taking into account additional damping of the plasma-resonance absorption according to the model of the mean-free-path effect. In Figure 5, the spectra of the five selected particles from Figure 1b are plotted. Peak position and magnitude of the G_1-mode obviously depend on the shape and size of the corresponding particle. The larger the eccentricity of the particle, the lower the wavenumber where the plasma-resonance absorption of the G_1-mode is peaked. The eccentricities, following from Table 1, are $e = 0.66$, $e = 0.41$, $e = 0.94$, $e = 0.83$ and $e = 0.98$ for particle 1 through 5. The peak magnitude approximately correlates with the particle volume, but for a quantitative comparison the dispersion of the optical constants in the polarizability must

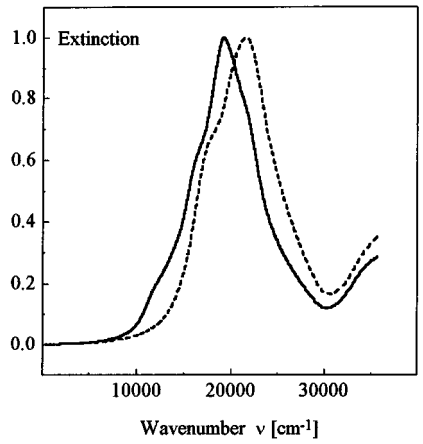

Fig. 6. Computed total extinction spectra for 368 particle before (straight line) and after (dashed line) reshaping. For better comparison, the spectra are normalized (Fig. 1).

be taken into account. For that reason, the absorption-peak magnitude of the larger particle 5 is smaller than the magnitude of particle 4, although its volume is larger than that of particle 4.

In Figure 6, finally, we present computed extinction spectra, for which the results from image analysis (Fig. 2) are used to compute extinction spectra of 368 particles with varying size parameters and adding them up to total spectra of the sample before (solid line) and after annealing (dashed line). For better comparison the spectra are normalized. It is obvious that the spectrum of the sample after annealing is blue-shifted with a shift of $\Delta\tilde{\nu}_r = 1570\ \mathrm{cm}^{-1}$. The peak positions before and after annealing are $\tilde{\nu}_r = 19\,420\ \mathrm{cm}^{-1}$ and $\tilde{\nu}_r = 21\,050\ \mathrm{cm}^{-1}$, in good agreement with our experimental data (Fig. 3). The halfwidths with $\Gamma = 7200\ \mathrm{cm}^{-1}$ and $\Gamma = 6730\ \mathrm{cm}^{-1}$ are larger than the measured halfwidths. One possible reason may be that the computed spectra exhibit resonances at lower wavenumbers which are missing in the measured spectra in Figure 3. They are caused by the restricted validity of the model used in our computations. As for silver particles with sizes exceeding about 20 nm the Rayleigh approximation becomes unvalid, more precise computations are needed. However, for ellipsoidal particles numerical problems prevented the application of the rigorous solution of Asano and Yamamoto [28], restricting numerical calculations on the used formula in the Rayleigh approximation.

4 Summary

In this paper, the optical extinction of plasma-polymer films with embedded silver particles was examined. As the optical properties of thin films with metal particles depend on the size and shape of the particles, we analyzed a sample by transmission electron microscopy in connection with optical image processing. In this sample, the microstructure before and after reshaping caused by thermal annealing was present in adjacent regions. This was achieved by electron-beam irradiation of a part of the sample in the TEM while other parts remained unirradiated during *in situ* annealing. The electron irradiation has caused hardening of the polymer matrix and prevented reshaping in the affected areas. With the assumption of ellipsoidal particles we got the major and minor half axis for 368 particles in the as-deposited part, and for 368 in the sample part after reshaping. We used these values in the model of Gans [15] for ellipsoidal particles to compute the extinction spectrum for each analyzed particle. The resulting sums over all extinction spectra of the single particles in both sample parts are in good agreement with the corresponding optical extinction spectra.

The agreement is better than found in computations with effective medium theories [5,26]. They also gave a good explanation of the peak position and the blue shift of the plasma-resonance absorption, but the halfwidth was much too low. In the computations with the Rayleigh-Gans theory the values for major and minor half axes were used for each single particle. There is an excellent coincidence of computed and experimental extinction spectra not only with respect to the spectral position, but also for the halfwidth of the plasma-resonance absorption. Additionally, the spectral blue shift caused by reshaping of the silver particles was confirmed.

To our knowledge, the Rayleigh-Gans theory was used for the first time to compute the optical extinction of an assembly of silver particles with experimentally determined particle sizes and shapes. In a forthcoming article we will extend our calculations to silver particles assemblies with different mean particle diameters and to embedded gold and indium particles.

The Deutsche Akademie der Naturforscher Leopoldina and the Innovationskolleg "Methods and materials for the nanometer region" at the Technical University Chemnitz-Zwickau are gratefully acknowledged for financial support.

References

1. H. Yasuda, *Plasma Polymerization* (Academic Press Orlando, 1985).
2. Y. Kagami, K. Yamada, T. Yamauchi, J. Gong, Y. Osada, Y., J. Appl. Polym. Sci., Appl. Polym. Symp. **46**, 289 (1990).
3. H. Yasuda, T.J.O. Keefe, D.L. Cho, B.K. Sun, Polym. Mat.: Sci. Engn. **62**, 524 (1990).
4. H. Biederman, L.Martinu, *Plasma Deposition, Treatment, and Etching of Polymers*, edited by R. d'Agostino (Academic Press San Diego, 1990).
5. A. Heilmann, J. Werner, O., Stenzel, F. Homilius, Thin Solid Films **246**, 77 (1994).
6. A. Heilmann, J. Werner, Thin Solid Films **317**, 21 (1998).
7. P.B. Comita, E. Kay, R. Zhang, W. Jacob, Appl. Surf. Sci. **79/80**, 196 (1994).
8. P.B. Comita, W. Jacob, E. Kay, R. Zhang, SPIE Proc. **1804** 154 (1993).
9. J. Werner, A. Heilmann, V. Hopfe, F. Homilius, B. Steiger, O. Stenzel, Thin Solid Films **237**, 193 (1994).

10. A. Heilmann, J. Werner, F. Homilius, F. Müller, J. Adhesion Sci. Technol. **9**, 1181 (1995).
11. J. Werner, A. Heilmann, F. Müller, Appl. Phys. Lett. **66**, 3426 (1995).
12. U. Kreibig, M. Vollmer, *Optical Properties of Metal Clusters*, Springer Series in Material Science 25 (Springer Berlin, 1995).
13. G. Mie, Ann. Phys. **25**, 377 (1908).
14. C.F. Bohren, D.R. Huffman, *Absorption and Scattering by Small Particles* (Wiley, New York, 1983).
15. R. Gans, Ann. Phys. **37**, 881 (1912).
16. A. Heilmann, C. Hamann, Prog. Coll. Polym. Sci. **85**, 102 (1991).
17. W. Grünewald, A. Heilmann, C. Reinhardt, Appl. Surf. Sci. **93**, 157 (1996).
18. A. Heilmann, J. Werner, M. Kelly, B. Holloway, E. Kay, Appl. Surf. Sci. **115**, 365 (1997).
19. J. Werner, Ph.D. Thesis, Technical University Chemnitz-Zwickau, 1996.
20. J. Perrin, B. Despax, E. Kay, Phys. Rev. B **32**, 719 (1985).
21. E. Kay, Z. Phys. D, **3**, 251 (1986).
22. A. Heilmann, A.-D. Müller, J. Werner, Surf. Rev. Lett. **3**, 1113 (1996).
23. A. Heilmann, J. Werner, D. Schwarzenberg, S. Henkel, P. Grosse, W. Theiß, Thin Solid Films **270**, 103 (1995).
24. A. Heilmann, J. Werner, V. Hopfe, Z. Phys. D **26S**, 39 (1993).
25. J.C. Garnett, Maxwell, Philos. Trans. Royal Soc. London **203**, 385 (1904); **205**, 237 (1906).
26. A. Heilmann, G. Kampfrath, V. Hopfe, J. Phys. D **21**, 986 (1988).
27. A.-D. Müller, A. Heilmann, F. Müller, Thin Solid Films **281-282**, 112 (1996).
28. S. Asano, G. Yamamoto, Appl. Opt. **14** 29 (1975).
29. W. Seitz, Ann. Phys. **21**, 1013 (1906).
30. W. von Ignatowski, Ann. Phys. **18**, 495 (1905).
31. R. Fuchs, Phys. Rev. B **11**, 1732 (1975).
32. M. Quinten, Z. Phys. B **101**, 211 (1996).